Appl. Magn. Reson. 14, 367–379 (1998)

Applied Magnetic Resonance

Anomalous Pulse-Angle and Phase Dependence of Hahn's Electron Spin Echo and Multiple-Quantum Echoes of the Spin Correlated Radical Pair $P700^+A_1^-$ in Photosystem I

H. Hara[1], J. Tang[2], A. Kawamori[1], S. Itoh[3], and M. Iwaki[3]

[1] Faculty of Science, Kwansei Gakuin University, Nishinomiya, Japan
[2] Chemistry Division, Argonne National Laboratory, Argonne, Illinois, USA
[3] National Institute for Basic Biology, Okazaki, Japan

Received June 15, 1997; revised March 13, 1998

Abstract. In a spin-correlated radical pair system, anomalous pulse-angle and phase dependence of electron spin echo and multiple-quantum echoes were theoretically calculated by Tang *et al.* (J. Chem. Phys. **106**, 7471 (1997)). The maximum intensity of the out of phase signal at 45 degree of spin rotation angle was experimentally verified in two-pulse echoes of the light-induced $P700^+A_1^-$ radical pair in Photosystem I. The values, $D = 1.64$ G and $J = 0.00$ G, fit well with the experimental ESEEM spectra. Single and double quantum echoes were observed at the value of $t = \tau$ and $T = 2\tau$ with the laser flash–t–$P1_{70,\xi1}$–τ–$P2_{140,\xi2}$–T *pulse sequence*, which led to determination of the relaxation time T_{23} between the singlet and triplet $|T_0\rangle$ states. The relaxation times of the zero and single quantum transitions were determined $T_{23} \approx 100$ ns and $T_2 = 1000$ ns, respectively. The field sweep ESE signal shape can be fitted with the hyperfine inhomogeneities of 7 G for $P700^+$ and of 10 G for A_1^-.

1. Introduction

Primary charge separation and subsequent electron transfer processes in natural and artificial photosynthetic reactions often lead to formation of radical pairs that exhibit unusual spin polarization (for review see [1]) The unpaired electron spins interact with each other by exchange and/or dipolar couplings and also with surrounding nuclear spins through hyperfine interactions. Electron spin echo (ESE) has been a useful technique in probing their magnetic interactions and kinetics. Because of a singlet-triplet mixing mechanism as well as the photoinduced zero-quantum coherence and initial non-Boltzmann populations of a spin correlated radical pair system, interesting and unusual transient phenomena can be observed [2–6] in addition to the well-known spin polarized CW EPR spectra. In pulsed

EPR, these methods originally were predicted theoretically for exchange and dipolar interacting radical pair systems by Salikhov *et al.* [2]. The out of phase ESEEM was first observed by Moënne-Loccoz *et al.* in PS I [7]. The direct determination of the dipolar and spin exchange interaction constants for a spin correlated radical pair was suggested by a theoretical study of the out-of-phase electron spin echo envelope modulation (ESEEM) [3]. The ESEEM spectra of the radical pair were observed in a bacterial RC by Dzuba *et al.* [6]. Both exchange and dipolar interactions have been first derived, and the distance between P860, the primary electron donor, and Q_A, the primary electron acceptor quinone, in a bacterial RC was found to be 26 Å [6]. The obtained value for the distance P860-Q_A is consistent with the X-ray data [8]. Later the correct distance between P700 and A_1 in PS I was derived by further experiments [4, 9]. The distance between P700, the primary electron donor, and A_1, the acceptor quinone, in PS I RC [4] was also determined to be 25 Å, which had not been derived by X-ray analysis because of the low resolution [10]. Applying a (laser flash–t–P1–τ–P2–T) pulse sequence, an additional second echo signal was found at $T = 2\tau$ for $t = \tau$ in the bacterial RC [5]. This second echo signal was assigned to a double-quantum echo.

In this paper we report some observed anomalies in a photoinduced radical pair in PS I RC using a two-pulse experiment after a laser flash to verify the theoretical derivation developed by Tang *et al.* [11]. The observed $P700^+A_1$ radical pair signal in PS I had manifested very high intensity, which was suitable to observe the various phenomena based on the theoretical study in [11]. We studied the dependence of the single-quantum spin echo on the spin rotation angle of the first pulse and the double-quantum echo signal on the phase angles of the first and the second pulses. Each spectra were well simulated with both in- and out-of-phase Hahn echo and double quantum echo and the spin relaxation time between singlet and triplet levels was estimated. Furthermore, we observed field sweep spectra in two-pulse sequence experiments and the obtained spectra were compared with theoretical simulations taking a nuclear hyperfine inhomogeneity into consideration.

2. Theory

In a radical pair system, the spin Hamiltonian for the rotating frame with angular frequency of Ω is given by [3] in unit of $\hbar$

$$\begin{aligned}\mathcal{H} = {} & (g_1\beta B_0 - \Omega)S_{1z} + (g_2\beta B_0 - \Omega)S_{2z} + S_{1z}\sum A_{1j}I_{jz} + S_{2z}\sum A_{2j}I_{jz} \\ & + J(1/2 - 2\mathbf{S}_1\mathbf{S}_2) + D(3\cos^2\theta - 1)\left(S_z^2 - S(S+1)/3\right)/2 \ , \end{aligned} \tag{1}$$

where β is the Bohr magneton and B_0 is the static magnetic field ($\| z$ axis of the laboratory frame). g_1 and g_2 are the effective g-tensor of $P700^+$ and A_1^-, $\mathbf{S}_1$

and $\mathbf{S}_2$ are their electron spin operators. A_{1j} and A_{2j} are z-components of their hyperfine interaction tensors with the j-th nuclear spin operator $\mathbf{I}_j$.

D represents the dipolar coupling constant, and θ is the angle between the line connecting the radical pair and the direction of the external magnetic field. $\mathbf{S} = \mathbf{S}_1 + \mathbf{S}_2$ is the resultant spin, and J is the spin exchange interaction constant. We will repeat a part of the previous result [11] for comparison of experimental results with theoretical simulations.

Using basic spin functions $|T_+\rangle$, $|T_-\rangle$, $|T_0\rangle$ for the triplet states and $|S\rangle$ for the singlet state, the two middle eigenstates $|\Phi_a\rangle$ and $|\Phi_b\rangle$ of the spin Hamiltonian Eq. (1) are a mixture of $|T_0\rangle$ and $|S\rangle$ caused by differences in g-factors and hyperfine interactions of $\mathbf{S}_1$ and $\mathbf{S}_2$,

$$\begin{aligned} |\Phi_a\rangle &= \cos\varphi|S\rangle + \sin\varphi|T_0\rangle \ , \\ |\Phi_b\rangle &= -\sin\varphi|S\rangle + \cos\varphi|T_0\rangle \ , \\ \tan 2\varphi &= \Delta\omega/\left(2J + D(3\cos^2\theta - 1)/3\right) \ . \end{aligned} \tag{2}$$

$\Delta\omega$ is the difference of resonance frequencies of the two spins in the absence of dipolar and exchange interactions,

$$\Delta\omega = (g_{1z} - g_{2z})\beta B_0 + \sum_i A_{1i}m_i - \sum_j A_{2j}m_j \ , \tag{3}$$

where $m_{i,j}$ is the magnetic quantum number of i or j-th nucleus. A Gaussian distribution of the nuclear hyperfine fields with a different second moment is assumed for each of $\sum_i A_{1i}m_i$ and $\sum_j A_{2j}m_j$. Equation (3) will be also used for simulation of the line shape observed in the field sweep spectra.

The eigenvalues of the Hamiltonian $\mathscr{H}$ are given by

$$\begin{aligned} E_1 &= \langle T_+|\mathscr{H}|T_+\rangle = (g_1 + g_2)\beta B_0/2 - \Omega + D(3\cos^2\theta - 1)/6 \ , \\ E_2 &= \langle \Phi_a|\mathscr{H}|\Phi_a\rangle = J - D(3\cos^2\theta - 1)/6 \\ &\quad + \frac{1}{2}\left[\left(2J + D(3\cos^2\theta - 1)/3\right)^2 + (\Delta\omega)^2\right]^{1/2} \ , \\ E_3 &= \langle \Phi_b|\mathscr{H}|\Phi_b\rangle = J - D(3\cos^2\theta - 1)/6 \\ &\quad - \frac{1}{2}\left[\left(2J + D(3\cos^2\theta - 1)/3\right)^2 + (\Delta\omega)^2\right]^{1/2} \ , \\ E_4 &= \langle T_-|\mathscr{H}|T_-\rangle = -(g_1 + g_2)\beta B_0/2 - \Omega + D(3\cos^2\theta - 1)/6 \ . \end{aligned} \tag{4}$$

In an ESE experiment, where the pulse sequence is given by (laser flash–t–P1$_{\zeta,\xi1}$–τ–P2$_{\zeta,\xi2}$–τ–echo), the out-of-phase signal $F_x(t, \tau)$ and the in-phase signal $F_y(t, \tau)$

corresponding to the transverse magnetization at the time τ after the 180° pulse are given by

$$\begin{aligned} F_x(t,\tau) &= \mathrm{Tr}[S_x \exp(-\mathrm{i}\mathscr{H}\tau) p_{180,0} \exp(-\mathrm{i}\mathscr{H}\tau) \\ &\quad \times p_{\zeta,\xi}\rho(t) p_{\zeta,\xi}{}^{\dagger} \exp(\mathrm{i}\mathscr{H}\tau) p_{180,0}{}^{\dagger} \exp(\mathrm{i}\mathscr{H}\tau)] \ , \\ F_y(t,\tau) &= \mathrm{Tr}[S_y \exp(-\mathrm{i}\mathscr{H}\tau) p_{180,0} \exp(-\mathrm{i}\mathscr{H}\tau) \\ &\quad \times p_{\zeta,\xi}\rho(t) p_{\zeta,\xi}{}^{\dagger} \exp(\mathrm{i}\mathscr{H}\tau) p_{180,0}{}^{\dagger} \exp(\mathrm{i}\mathscr{H}\tau)] \ , \end{aligned} \tag{5}$$

where the pulse rotation angle ζ and the pulse phase ξ of the first pulse $\mathrm{P}_{\zeta,\xi 1}$ can be arbitrary, whereas the pulse rotation and phase angles for the second pulse $\mathrm{P}_{180,0}$ are fixed. † means Hermitian-conjugate. Finally Eqs. (5) are summarized by following relations [11]:

$$\begin{aligned} F_x(t,\tau) &= \cos\xi\,[A_1(t,\tau) + A_2(t,\tau)] \ , \\ F_y(t,\tau) &= \sin\xi\,[A_1(t,\tau) + A_2(t,\tau)] \ , \\ A_1(t,\tau) &= \sin\zeta \sin^2 2\varphi \cos 2\varphi \exp(-2\tau/T_2)(\cos E_{23}\tau - 1) \\ &\quad \times \Big[\exp(-t/T_{23}) \sin E_{23} t \cos(E_1 + E_4 - E_2 - E_3)\tau \\ &\quad + \cos 2\varphi \big(1 - \exp(-t/T_{23}) \cos E_{23} t\big) \sin(E_1 + E_4 - E_2 - E_3)\tau\Big] \ , \\ A_2(t,\tau) &= (1/2) \sin 2\zeta \sin^2 2\varphi \exp(-2\tau/T_2)\big(\exp(-t/T_{23}) \cos E_{23} t - 1\big) \\ &\quad \times \Big[\cos 2\varphi \sin E_{23}\tau \cos(E_1 + E_4 - E_2 - E_3)\tau \\ &\quad + \sin^2 2\varphi + \cos^2 2\varphi E_{23}\tau \sin(E_1 + E_4 - E_2 - E_3)\tau\Big] \ , \end{aligned} \tag{6}$$

where $E_{23} = E_2 - E_3$. T_{23} is the phase memory time for the photo induced zero-quantum coherence between the energy levels E_2 and E_3 and T_2 is that for four single quantum transitions with frequencies E_{12}, E_{13}, E_{24} and E_{34}. If the phase ξ for the first pulse P1 is 0, i.e., along the x axis, one can easily see from the above equation that $F_y(t,\tau) = 0$ [2, 3]. The observed time T dependence of $F_x(t,\tau,T)$ and $F_y(t,\tau,T)$ can be calculated for the density matrix given in [11] by Eq. (5) and represented by a little modification:

$$\begin{aligned} F_x(t,\tau,T) &= \mathrm{Tr}[S_x \exp(-\mathrm{i}\mathscr{H}T) p_{180,0} \exp(-\mathrm{i}\mathscr{H}\tau)(t,\tau) \\ &\quad \times p_{\zeta,\xi}\rho(t) p_{\zeta,\xi}{}^{\dagger} \exp(\mathrm{i}\mathscr{H}\tau) p_{180,0}{}^{\dagger} \exp(\mathrm{i}\mathscr{H}T)] \ , \\ F_y(t,\tau,T) &= \mathrm{Tr}[S_y \exp(-\mathrm{i}\mathscr{H}T) p_{180,0} \exp(-\mathrm{i}\mathscr{H}\tau) \\ &\quad \times p_{\zeta,\xi}\rho(t) p_{\zeta,\xi}{}^{\dagger} \exp(\mathrm{i}\mathscr{H}\tau) p_{180,0}{}^{\dagger} \exp(\mathrm{i}\mathscr{H}T)] \ . \end{aligned} \tag{7}$$

We have so far considered an ideal case using strong pulses that cover the whole spectral width. To apply an arbitrary microwave power to the two pulse experiment, we have used a numerical calculation of Eq. (5). For a correct simulation of ESEEM, however, the finite pulse strength and duration should be taken into account as used later for simulation of the field sweep spectra.

3. Experimental

PS I membranes were isolated from spinach by the method of Iwaki and Itoh [12]. The PS I RC contained P700, A_0, A_1, iron-sulfur centers (F_X, F_A and F_B) as electron transfer components and about 20 molecules of antenna chlorophyll [13]. Glycerol was added to the membranes up to the concentration of 60% (v/v) to improve the illumination efficiency. The concentration of RC in the sample was about 20 μM. The membranes were loaded into Suprasil quartz tubes with the inner diameter of 4 mm and the height of 10 mm. The samples have been stored in liquid N_2 until measurements.

The ESE experiments of the spin polarized radical pair in PS I have been performed on a Fourier transform pulsed EPR spectrometer Bruker ESP-380 equipped with a dielectric cavity (Bruker ER 4117 DHQ-H) and a cold gas flow cryostat (Oxford Instruments CF935). The cavity Q-value was adjusted to provide a spectrometer dead time of 100 ns. To acquire a two-pulse echo signal, two microwave pulses were created at two pulse former channels. The pulse length of these pulses was same and adjusted to 32 ns, while the amplitude was varied to change the spin rotation angle. For pulse rotation angle study, the transient states were detected with pulse sequences (laser flash–t–$P1_{\zeta,0}$–τ–$P2_{180,0}$–T) and for the double quantum echo study with (laser flash–t–$P1_{\zeta,\xi 1}$–τ–$P2_{2\zeta,\xi 2}$–T), respectively. For the ESEEM and field sweep experiments, 45° for P1 pulse was applied, because the theoretical derivation predicts the maximum ESE intensity [11, 14]. ζ is the pulse rotation angle and ξ, the pulse phase. For calibration of pulse phases, the Cr^{3+} (g = 1.9800, S = 3/2) in MgO was loaded in the capillary tubes, and then inserted into the sample tube of PS I. Cr^{3+} echo intensity of in-phase signal was calibrated versus phase angles. The absolute pulse levels of the two in-phase and out-of-phase pulse channels were calibrated by the FID signal of DPPH (1,1-diphenyl-2-picryl-hydrazyl).

The PS I RCs were excited with 4 ns FWHM flashes from a Continuum Surelite I Nd:YAG laser equipped with an optical parametric oscillator (OPO). The excitation wave length was adjusted to about 700 nm. The microwave pulses and laser pulses were triggered externally by a Digital Delay/Pulse Generator (Stanford Research Systems, model DG135) at a repetition rate of 10 Hz generated by a personal computer (IBM Aptiva 730). The jitters of the laser flashes and microwave pulses were less than 1 ns. The magnetic field was fixed to give the maximum echo amplitude. 1000 shots echo shapes were accumulated with a LeCroy 9400A 175 MHz digital storage oscilloscope (10 ns resolution per point). The field sweep ESE was obtained with a boxcar gate average and a signal processor (EG&G Princeton Applied Research, Model 4420 & 4402).

4. Results and Discussion

The spin polarized radical pair signals were observed using the quadrature detection with both in and out-of-phases. The amplitudes of the signals character-

ized by the spin polarized radical pair were independent of temperature as expected. All measurements were performed at a temperature of 80 K.

4.1. Dependence on the Pulse Rotation Angle ζ of the Echo Amplitude Observed with a Laser Flash–t–$P1_{\zeta,0}$–τ–$P2_{180,0}$ Pulse Sequence

The dependences of the echo amplitude on the pulse rotation angle ζ of the first microwave pulse were shown in Fig. 1. For an ordinary Hahn's echo with an initial Boltzmann distribution, the maximum echo amplitude is usually created at $\zeta = 90°$. However, for the spin polarized system, the first maximum was observed at about 45° and the second maximum with negative sign at about 135° of ζ as shown by Tang *et al.* [11, 14, 15]. In Eq. (6) the out-of-phase echo amplitude includes dependencies on $\sin\zeta$ and $\sin 2\zeta$. The $\sin\zeta$-dependence has been derived from $\langle S|\rho(t)|T_0\rangle$, while the $\sin 2\zeta$-dependence, from $\langle S|\rho(t)|S\rangle$ and $\langle T_0|\rho(t)|T_0\rangle$. Due to the ensemble average of multiple nuclear spin configurations, the oscillation of the populations between $\langle S|\rho(t)|T_0\rangle$ and $\langle T_0|\rho(t)|T_0\rangle$ is highly damped. The ensemble average of $F(t)$ (including $\langle S|\rho(t)|T_0\rangle$ term) is usually smaller than that of $G(t)$ (including $\langle T_0|\rho(t)|T_0\rangle$ term) so that the echo amplitude has $\sin 2\zeta$ dependence as a major contribution. The strongest out-of-phase echo, therefore, is expected to occur for about 45° and 135° of the pulse angle ζ. The closed and open circles in Fig. 1 show the echo amplitudes versus ζ value for $\tau = 120$ ns and $\tau = 264$ ns, respectively. These data points are in good agreement with the theoretical calculation (see Fig. 3 in [11]). Figure 2a shows the observed spin polarized ESEEM spectra (solid curve) with $\zeta = 45°$ and the simulated curve (dotted line) for PS I RC. In this simulation, the parameters $J = 0.00$ G, $D = 1.64$ G and $(g_1 - g_2)\beta B_0 = 6.8$ G, and $T_2 = 1000$ ns

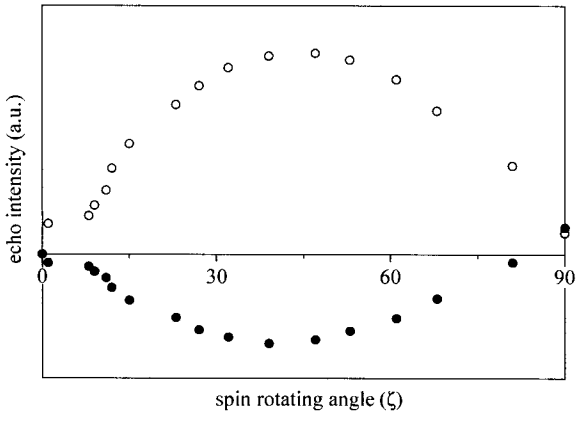

Fig. 1. The dependence of the echo amplitude on the spin rotation angle ζ by the first microwave pulse P1 at $t = 1000$ ns. The open circles show the echo amplitude observed at $\tau = 120$ ns and closed circles, that at 264 ns. Measurement conditions: microwave frequency, 9.6 GHz; magnetic field, 3450 G; temperature, 80 K; the pulse duration time, 32 ns.

and T_{23} = 100 ns were used in Eq. (6). The effect of T_2 and T_{23} has not been taken into consideration in our previous analysis [4]. The square root of the second moment of the hyperfine field at each electron spin is taken to be 7 G and 10 G, respectively. In this simulation, the differences of the g-anisotropies and T_{23} values affect little on the spectral shapes. Taking into account the experimental accuracy, the dipolar, exchange interaction and relaxation time were

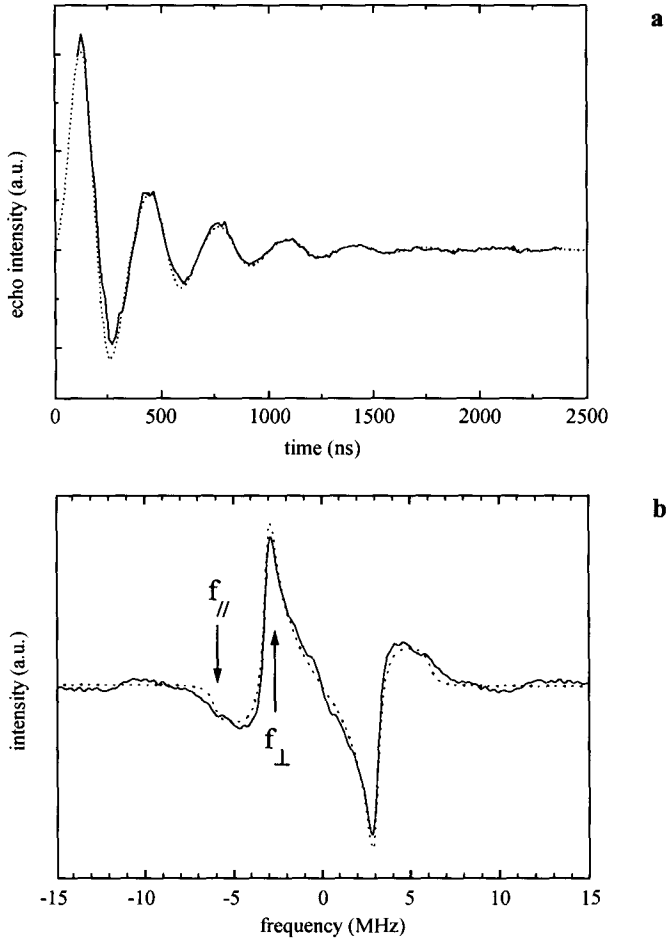

Fig. 2. **a** Two-pulse echo signal intensity as a function of the time separation τ between the first and second microwave pulses. **b** The sine Fourier transformation of the time domain data. The solid curve shows the experimental data observed at 80 K in PS I RC and the dotted line shows the simulation curve based on Eq. (6) and a Gaussian line broadening. The parameters J = 0.00 G, D = 1.64 G, $(g_1 - g_2)\beta B_0$ = 6.8 G, T_2 = 1000 ns were used in Eq. (6) (see text). The square root of the second moment of the hyperfine field at each electron spin is assumed to be 7 G and 10 G, respectively. In the left half-part of the frequency domain spectrum (**b**), the frequencies $f_\perp$ and $f_{//}$ are indicated. The solid curve shows the experimental data and the dotted line shows the simulated values based on Eq. (6). Measurement conditions: the same as in Fig. 1.

determined as $J = 0.00 \pm 0.01$ G, $D = 1.64 \pm 0.05$ G and $T_2 = 1000 \pm 100$ ns, respectively. To obtain a smooth curve with sufficient ensemble averaging, 100 angles for the dipolar field and 60 discrete values with a Gaussian distribution for each hyperfine field were used. The modulation pattern of the out of phase signal is caused by the $E_1+E_4-E_2-E_3$ terms in Eq. (6) [3]. These terms depend on only dipole D and exchange J interactions but neither on hyperfine interactions nor on differences in g-values. This result shows that the ESEEM signal of the spin polarized radical can be used to determine the dipolar and/or spin exchange interaction directly, though such small interaction has been difficult to observe by a CW method. The results of Fourier transformation of Fig. 2a are shown in Fig. 2b. The solid curve shows the experimental data and the dotted line shows the simulation points. There are two pronounced peaks seen in the Fourier transformed spectra. These peaks correspond to singularities occurring for the perpendicular orientation of the line connecting the two radicals with respect to the magnetic field ($\theta = 90°$). The spectral edge corresponds to the parallel orientation ($\theta = 0°$). These spectral peaks and edges are given by following equations [6]:

$$f_\perp = \pm(2D/3 + 2J) ,$$
$$f_\parallel = \pm(-4D/3 + 2J) . \quad (7)$$

These formula depend only on D and J values. The obtained frequencies are $f_\perp = 3.06$ and $f_\parallel = 6.12$ MHz, respectively. In our previous study, we determined the spectral peaks and edges are $f_\perp = 3.0$ and $f_\parallel = 6.2$ MHz, respectively [4]. These values correspond to the interaction values $D = 1.71 \pm 0.05$ G and $J = -0.01 \pm 0.015$ G. Independently, Bittl *et al.* determined D to be 1.70 ± 0.04 G and J to be -0.01 ± 0.005 G, respectively [9]. Taking into account the determined comparatively large distance between P700 and A_1, i.e., 25 Å, the exchange interaction should be zero, which resulted in the smaller value of D in this work.

4.2. The Double-Quantum Echo Observed with Two Microwave Pulses

Possibility for detection of zero-, single- and double-quantum signals in the spin correlated radical pair by varying the pulse phase has been suggested by Tang *et al.* [16]. Using the pulse sequence (laser flash–t–$P1_{\zeta,\xi}$–τ–$P2_{2\zeta,\xi 2}$–T), a double-quantum echo has been observed at $t = \tau$ and $T = 2\tau$ in the $P860^+Q_A^-$ radical pair by Dzuba *et al.* [5]. According to the numerical calculation [11], the pulse angle dependence of the double-quantum echo is given by $\sin 2\zeta(1 - \cos 2\zeta)^2$, which has a maximum for 69.3°. This echo is originated from the photoinduced zero-quantum coherence that is converted into a double-quantum coherence by the first microwave pulse. In an ordinary NMR or EPR with Boltzmann spin population, a spin state coherence is created only through radio frequency irradiation. However, in this photoinduced radical pairs the zero-quantum coherence can be cre-

ated by a laser excitation. When the time interval t between the laser flash and the first pulse is varied, this double-quantum echo disappears outside the region $(0.9–1.1)\tau$. It indicates that this secondary echo truly originates from the photoinduced zero-quantum coherence between Φ_a and Φ_b states, whereas the population difference between Φ_a and Φ_b states results in the out-of-phase Hahn echo. The experimental results show that the Hahn echo does not diminish in intensity, when one increases the time interval t between the laser and the first pulse up to 20 μs. The Hahn echo signal decays after the order of T_2 (≈30 μs [4]). If the Hahn echo were caused by the photoinduced coherence between these two states, it would decay much faster within the order of T_{23}. A density matrix calculation also shows that the initial coherence right after the laser pulse can not be refocused and therefore would not contribute to the formation of the Hahn echo.

Observation of this second echo is experimentally difficult because of its weak intensity. The second echo amplitude is governed by three relaxation rates; T_2 for single-quantum coherence, T_{23} for zero-quantum coherence and T_{14} for double-quan-

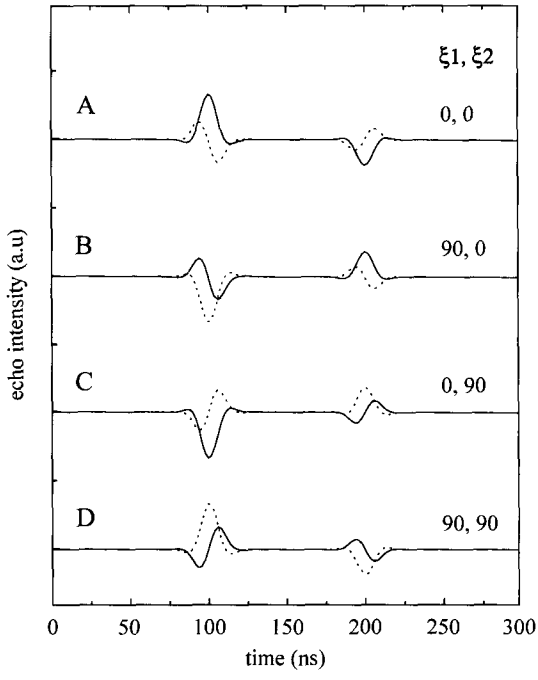

Fig. 3. The time T dependence of simulations $F_x(t, \tau, T)$ (solid curve) and $F_y(t, t, T)$ (dotted line) for two pulse sequence using Eq. (7). The pulse sequence (laser flash–t–P1$_{\zeta,\xi1}$–τ–P2$_{2\zeta,\xi2}$–T) with $t = \tau = 100$ ns and $\zeta = 70°$ was used. The phases of two pulses ($\xi1$, $\xi2$) are A (0°, 0°), B (90°, 0°), C (0°, 90°) and D (90°, 90°), respectively. The dependence on pulse phases ($\xi1$, $\xi2$) of two pulses indicates that the second echo at $T = 2\tau$ is assigned to appearance of the double-quantum coherence that has evolved between the first and the second pulse, whereas the first echo at $T = \tau$ is assigned to the single-quantum coherence in the evolution period τ.

tum coherence. The relaxation of double-quantum coherence occurs between $|T_+\rangle$ and $|T_-\rangle$ that have been populated by the first microwave pulse P1 [11]. Figure 3 shows the time profiles of T, in which the first echo at $T = \tau$ and the second echo at $T = 2\tau$ were obtained by the simulation with $J = 0.00$ G, $D = 1.64$ G, $(g_1 - g_2)\beta B_0 = 6.8$ G and $\tau = 100$ ns using Eq. (7). The pulse angle was $\zeta = 70°$ and the phases of two pulses ($\xi 1$, $\xi 2$) are curve A, (0°, 0°), curve B, (90°, 0°), curve C, (0°, 90°) and curve D, (90°, 90°), respectively. The square root of the second moment of the hyperfine field at each electron spin is assumed to be 7 G and 10 G, respectively, though these values do not affect the time profiles of these echo shapes. The calculated time profile coincided with that given by the previous work [11].

The second echo is assigned to the double-quantum coherence. The shape of the second echo is inverted (180° degree phase shift) due to 90° phase shift of $\xi 1$ applied by the first pulse with $\zeta = 70°$. On the other hand, the first echo is inverted due to 90° phase shift of $\xi 2$ applied by the second pulse with $2\zeta = 140°$ [6]. Figure 4 shows experimental results of the first and second echo signal shapes obtained for $t = \tau = 120$ ns (Fig. 4a) and $t = \tau = 264$ ns (Fig. 4b), respectively. The phases of two pulses ($\xi 1$, $\xi 2$) are curves A, (0°, 0°), curves B, (90°, 0°), curves C, (0°, 90°) and curves D, (90°, 90°), respectively. The patterns of the first and second echo signals are in good agreement with the simulated curves

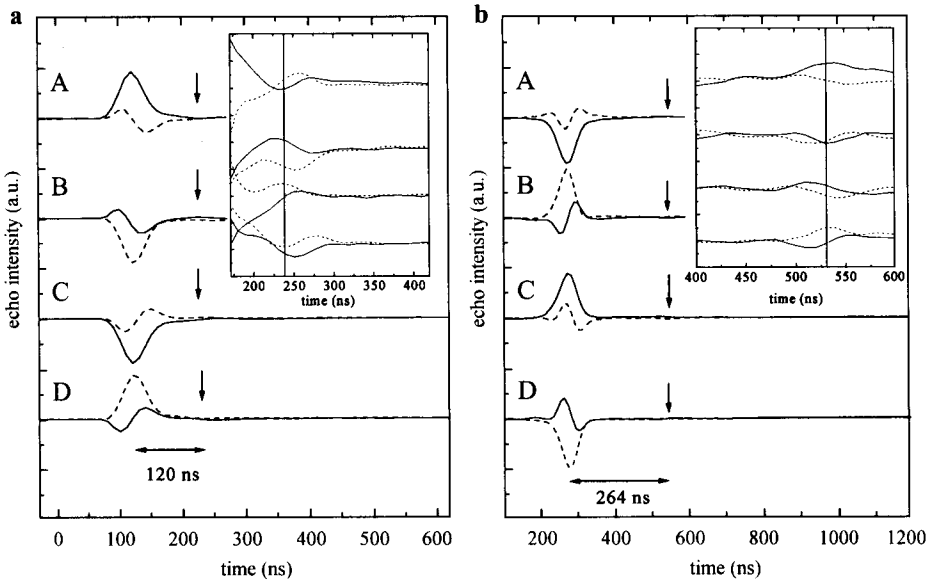

Fig. 4. The T dependence of experimental signals $F_x(t, \tau, T)$ (solid curve) and $F_y(t, \tau, T)$ (dotted line) observed for the two pulse sequence (laser flash–t–P1$_{\zeta,\xi 1}$–τ–P2$_{2\zeta,\xi 2}$–T) with $\zeta = 70°$. **a** $t = \tau = 120$ ns and **b** $t = \tau = 264$ ns, respectively. The phases of two pulses ($\xi 1$, $\xi 2$) are A (0°, 0°), B (90°, 0°), C (0°, 90°) and D (90°, 90°), respectively. The inset of each figure shows the enlarged spectra in the expanded time scale around the indicated arrows. Measurement conditions: the same as in Fig. 1.

shown in Fig. 3. However, the intensity of the second echo is considered to decrease by the factor of $\exp(-2\tau/T_2)\exp(-\tau/T_{23})\exp(-\tau/T_{14})$ from the calculated intensity in Fig. 3. In the simulation of the ESEEM in Fig. 2, these relaxation times T_2 and T_{23} have been taken into consideration. The estimated value of $T_2 = 1000$ ns obtained from the ESEEM decay curve was used in the simulation, which affects substantially on the line shape. On the other hand, T_{23} value does not significantly influence the spectral shape and $T_{23} = 1000$ ns was tentatively used. Then the time dependence for $\exp(-\tau/T_{23})\exp(-\tau/T_{14})$ can be estimated by comparison with the observed intensity of the second echo and the simulated one using Eq. (7). We can derive the value of $(1/T_{23} + 1/T_{14})^{-1} = 100 \pm 20$ ns from Fig. 4. This value for $P700^+A_1^-$ is much shorter than the value for the $P860^+Q_A^-$ radical pair ($\approx$350 ns) in bacterial RC [5]. The relaxation rate $1/T_{14}$ between $|T_+\rangle$ and $|T_-\rangle$ states may be neglected compared to $1/T_{23}$, because the energy difference between E_1 and E_4 is much larger than that between E_2 and E_3 and cross relaxation does not work on $1/T_{14}$. $T_{23} \approx 100$ ns could be derived. Thus, observation of the spin polarized ESEEM and double-quantum echo allows us to determine the spin relaxation time between the singlet and triplet states.

The multi-quantum echoes are also predicted for the three-pulse sequence in the theoretical calculation by Tang *et al.* [11]. However, the behavior of the multi-quantum echoes is more sensitive to the pulse phase and time interval between the laser and microwave pulses than that for the two-pulse sequence. We could detect only a broad response in the time domain, because of the low resolution due to the inhomogeneity of the actual pulse and/or a short relaxation time i.e., T_2.

4.3. The Field Sweep Spectrum with Two Microwave Pulses

The field sweep ESE spectrum for two-pulse sequences accumulated with a boxcar gate is shown in Fig. 5 (solid curve). This spectrum has about 8 G linewidth. In the two-pulse field sweep ESE, the resonance field is given by E_1-E_2, E_1-E_3, E_2-E_4 and E_3-E_4 in Eq. (4) and the spectrum linewidth is explained by E_2-E_3. As the dipolar and exchange interactions are relatively small in this case, and E_{23} is approximated by $(g_1 - g_2)\beta B_0 + (\sum_i A_{1i}m_i - \sum_j A_{2j}m_j)$ given by Eq. (3). The resonance position and the line shape are determined by the difference of g-values $(g_1 - g_2)\beta B_0$ and the nuclear quantum numbers, respectively. The g-values of $P700^+$ and A_1^- are taken from the result of CW EPR studied by van der Est *et al.* [17]. In calculation, the anisotropy in g-values did not influence any appreciable effect on the field sweep spectra in X-band compared with large hyperfine interaction values. Only average g-values were taken into consideration. A Gaussian distribution of the nuclear hyperfine fields with a different second moment is assumed for each of $\sum_i A_{1i}m_i$ and $\sum_j A_{2j}m_j$ in Eq. (1). For calculation, we took an ensemble average over 60 discrete values of $\sum_i A_{1i}m_i$ and $\sum_j A_{2j}m_j$. Dotted line in Fig. 5 shows the simulated values. The linewidths of $P700^+$ and A_1^- radicals were reported to be 7.2 ($g = 2.0025$) and 10.5

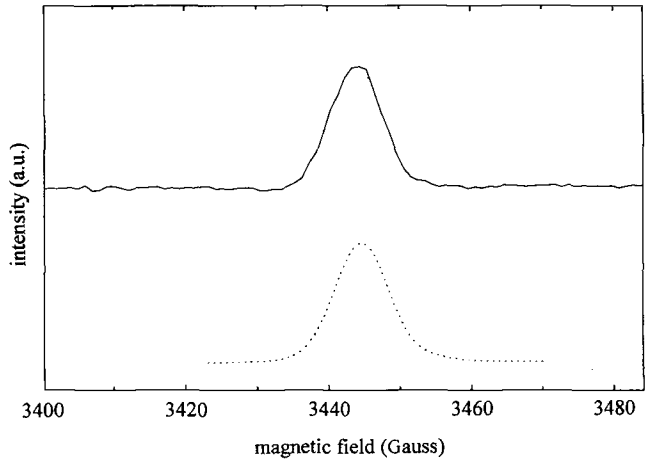

Fig. 5. Field sweep ESE spectra accumulated by a boxcar gate integrator with its gate width = 150 ns for a two-pulse sequence (solid curve), laser flash–t–$P1_{45.0}$–τ–$P2_{180.0}$ with t = 1000 ns and τ = 120 ns. The dotted line shows the simulated values with the square root of the second moment of the hyperfine field at each electron spin is taken to be 7 and 10 G for $P700^+$ and A_1^-, respectively (see text). Measurement conditions: the same as in Fig. 1 except for the magnetic field strength.

($g \approx 2.005$) G, respectively [18]. The simulation with the square roots of the second moment of the hyperfine fields 7 and 10 G for $P700^+$ and A_1^-, respectively, is found to be in good agreement with the experimental line shape.

In addition to the dipolar and exchange interaction parameters determined from the ESEEM experiments, we could derive information of broadening due to the hyperfine interaction from the field sweep ESE spectrum. In CW experiment the line shape is usually distorted by other emission spectra and difficult to determine the exact linewidth. Even zero-quantum beat frequencies observed in a time-resolved CW EPR are much less sensitive to these small dipolar and exchange interactions [19].

5. Conclusion

We have observed several anomalies in a photoinduced radical pair, $P700^+A_1^-$ in PS I, such as pulse rotation angle and phase dependence of Hahn's spin echo and multiple-quantum echoes. The anomalies were well simulated by the previous theoretical prediction using the parameters for g-value and hyperfine interactions of each radical and the weak dipolar and exchange interaction between them [11]. The ESEEM signal in a spin correlated radical pair provides useful structural information for the dipole and exchange interactions. When CW EPR is not enough resolved because of overlapping with emission spectra in a spin correlated radical pair system, the hyperfine field inhomogeneity can be derived from the field sweep spectra of the two-pulse echo.

Acknowledgements

J. T. acknowledges the support by the U.S. Department of Energy, Office of Basic Energy Sciences, Division of Chemical Science, under Contact W-31-109-Eng-38 and acknowledges the support by Kwansei Gakuin University travel fund for this international cooperation. This work is supported by the Kwansei Gakuin University private fund to A. K.

References

[1] Molin Y.: Spin Polarization and Magnetic Effects in Radical Reactions. Amsterdam: Elsevier 1984.
[2] Salikhov K.M., Kandrashkin Yu.E., Salikhov A.K.: Appl. Magn. Reson. **3**, 199 (1992)
[3] Tang J., Thurnauer M.C., Norris J.R.: Chem. Phys. Lett. **219**, 283 (1994)
[4] Dzuba S.A., Hara H., Kawamori A., Iwaki M., Itoh S., Tsvetkov Yu.D.: Chem. Phys. Lett. **264**, 238 (1997)
[5] Dzuba S.A., Bosch M.K., Hoff A.J.: Chem. Phys. Lett. **248**, 427 (1996)
[6] Dzuba S.A., Gast P., Hoff A.J.: Chem. Phys. Lett. **236**, 595 (1995)
[7] Moënne-Loccoz P., Heathcote P., Maclachlan D.J., Berry M.C., Davis I.H., Evans M.C.W.: Biochemistry **33**, 10037 (1994)
[8] Yeates T.O., Komiya H., Rees D.C., Allen J.P., Feher G.: Proc. Natl. Acad. Sci. USA **84**, 6438 (1987)
[9] Bittl R., Zech S.G.: J. Phys. Chem. B **101**, 1429 (1997)
[10] Fromme P., Witt H.T., Schubert W.D., Klukas O., Saenger W., Kraub N.: Biophys. Biochim. Acta **1275**, 76 (1996)
[11] Tang J., Thurnauer M.C., Kubo A., Hara H., Kawamori A.: J. Chem. Phys. **160**, 7471 (1997)
[12] Iwaki M., Itoh S.: FEBS Lett. **256**, 11 (1989)
[13] Itoh S., Iwaki M., Ikegami I., Biophys. Biochim. Acta **893**, 508 (1987)
[14] Tang J., Thurnauer M.C., Norris J.R.: Appl. Magn. Reson. **9**, 29 (1995)
[15] Hasharoni K., Levanon H., Tang J., Bowman M.K., Norris J.R., Gust D., Moore T.A., Moore A.: J. Am. Chem. Soc. **112**, 6477 (1990)
[16] Tang J., Norris J.R.: Chem. Phys. Lett. **233**, 192 (1995)
[17] Van der Est A., Prisner T., Bittl R., Fromme P., Lubitz W., Möbius K., Stehlik D.: J. Phys. Chem. B **101**, 1437 (1997)
[18] Staehelin L.A., Arntzen C.J.: Photosynthesis III. Berlin: Springer 1986.
[19] Kothe G., Weber S., Ohmes E., Thurnauer M.C., Norris J.R.: J. Phys. Chem. **98**, 2706 (1994)

Author's address: Prof. Asako Kawamori, Faculty of Science, Kwansei Gakuin University, Uegahara 1-1-155, Nishinomiya 662, Japan